Rheol Acta (2012) 51:511–526
DOI 10.1007/s00397-011-0610-x

ORIGINAL CONTRIBUTION

Laminar axisymmetric flow of a weakly compressible viscoelastic fluid

Kostas D. Housiadas · Georgios C. Georgiou · Ioannis G. Mamoutos

Received: 13 August 2011 / Revised: 2 November 2011 / Accepted: 30 November 2011 / Published online: 24 December 2011
© Springer-Verlag 2011

Abstract The combined effects of weak compressibility and viscoelasticity in steady, isothermal, laminar axisymmetric Poiseuille flow are investigated. Viscoelasticity is taken into account by employing the Oldroyd-B constitutive model. The fluid is assumed to be weakly compressible with a density that varies linearly with pressure. The flow problem is solved using a regular perturbation scheme in terms of the dimensionless isothermal compressibility parameter. The sequence of partial differential equations resulting from the perturbation procedure is solved analytically up to second order. The two-dimensional solution reveals the effects of compressibility and the other dimensionless numbers and parameters in the flow. Expressions for the average pressure drop, the volumetric flow rate, the total axial stress, as well as for the skin friction factor are also derived and discussed. The validity of other techniques used to obtain approximate solutions of weakly compressible flows is also discussed in conjunction with the present results.

K. D. Housiadas (✉) · I. G. Mamoutos
Department of Mathematics, University of the Aegean, Karlovassi, Samos, 83200, Greece
e-mail: housiada@aegean.gr

G. C. Georgiou
Department of Mathematics and Statistics, University of Cyprus, P.O. Box 20537, 1678 Nicosia, Cyprus

Present Address:
I. G. Mamoutos
Department of Marine Sciences, University of the Aegean, Mytilene, Lesvos, Greece

Keywords Pressure drop · Compressibility · Two-dimensional flow · Oldroyd-B fluid · Flow curve · Pipe flow

Introduction

The importance of compressibility in non-Newtonian viscous flows has been underlined in many studies during the last decades. A measure of the fluid compressibility is the Mach number, Ma, which is defined as the ratio of the characteristic speed of the fluid to the speed of sound in that fluid. A zero Mach number corresponds to incompressible flow, whereas for low Mach numbers ($Ma << 1$), the flow is considered as a weakly compressible one. Compressibility becomes significant in flows where the fluid is exposed to very high pressure differences, such as the extrusion process (Hatzikiriakos and Dealy 1992), injection blow molding, jet cutting, and liquid impact (Keshtiban et al. 2005), or in flows involving relatively long tubes (Vinay et al. 2006) or locally near sharp corners (Guillopé et al. 2005). Hatzikiriakos and Dealy (1992) demonstrated experimentally that the stick–slip polymer extrusion instability is caused by the combined effects of compressibility and non-linear slip. The same authors also noted that, although the isothermal compressibility of molten polymers is very small, it can have a very strong effect on the time required for the pressure to level off in a capillary flow experiment (Hatzikiriakos and Dealy 1994). Ranganathan et al. (1999) presented time-dependent experimental flow data in a capillary for a high-density polyethylene using the multipass rheometer and showed that the observed pressure relaxation

on cessation of the piston movement can be almost entirely attributed to the compressibility of the melt.

Numerical simulations of viscous compressible flows have been reported by various researchers in the past two decades. Georgiou and Crochet (1994a, b) performed numerical simulations of the time-dependent Newtonian extrudate-swell problem with slip at the wall in order to verify the compressibility/slip mechanism for the stick–slip instability, i.e., that the combination of compressibility and nonlinear slip leads to self-sustained oscillations of the pressure drop and of the mass flow rate in the unstable regime. They also pointed out that a very low fluid compressibility may not have an effect on steady-state solutions but can change dramatically flow dynamics. Taliadorou et al. (2007) presented similar simulations for a Carreau fluid and included the barrel region where the polymer melt is compressed and decompressed periodically. Guo and Wu (1997, 1998) presented certain numerical results for the non-isothermal flow of a compressible gas in a microtube by utilizing a simplified form of the governing equations. They used a finite difference forward marching procedure and found that fluid compressibility increases the skin friction coefficient. Valette et al. (2006) simulated time-dependent pressure driven flows for a polymer melt flowing within an entry and exit slit geometry using the Rolie-Poly constitutive model and reported that their simulation gave an accurate description of the experimental data. Moreover, the simulation predicted an initially unexpected time-dependent variation of the absolute pressure. Taliadorou et al. (2008) simulated the extrusion of strongly compressible Newtonian liquids and found that compressibility can lead to oscillatory steady-state free surfaces. Webster et al. (2004) introduced numerical algorithms for solving weakly compressible, highly viscous laminar Newtonian flows at low Mach numbers. They applied their methods to the driven cavity and the contraction flow problems. Subsequently, Keshtiban et al. (2004, 2005) and Belblidia et al. (2006) simulated the flow of weakly compressible Oldroyd-B fluids in entry–exit flows in high-pressure-drop cases.

Only a few approximate analytical solutions for compressible viscous flows in capillaries/tubes and channels have been reported in the literature. These have been obtained following three basic techniques. The first approach is the one-dimensional approximation in which cross-sectional averaged quantities and equations are considered (Shapiro 1953). Since non-linear terms are averaged, a closure of the resulting equations is necessary, which, however, introduces errors leading to erroneous predictions even at the leading order of the compressibility (Schwartz 1987).

The second technique is the lubrication approximation (Prud'homme et al. 1986; van den Berg et al. 1993; Harley et al. 1995; Zohar et al. 2002), valid for slow flows or flows in very long tubes and channels, so that both the velocity component and the pressure gradient in the transverse direction can be assumed to be zero. As will be demonstrated in the present work, these assumptions introduce errors similar to those of the one-dimensional technique.

The third technique is a regular perturbation procedure according to which the dependent flow variables are expanded as series solutions in terms of a small parameter related to the fluid compressibility (Schwartz 1987; Venerus 2006; Taliadorou et al. 2009a; Venerus and Bugajsky 2010; Housiadas and Georgiou 2011). The perturbation technique involves fewer assumptions than the other techniques and leads to two-dimensional expressions for the axial velocity and pressure in Poiseuille flow and to non-zero radial velocity.

The limitations of the one-dimensional and lubrication approximations for studying compressible Newtonian Poiseuille flows were pointed out by Schwartz (1987), who solved the weakly compressible Newtonian flow in a channel by using a fourth-order perturbation scheme based on the principle of slow variation. He also assumed a zero bulk viscosity and that the mass density of the fluid was proportional to the pressure (thermally perfect gas). The first two-dimensional asymptotic solution for weakly compressible Newtonian flow in a capillary was presented by Venerus (2006), who used a streamfunction/vorticity formulation and a regular perturbation scheme with the small parameter being the dimensionless isothermal compressibility parameter to obtain a solution up to second order. More recently, Taliadorou et al. (2009a) proposed an analogous perturbation scheme, but in a velocity/pressure formulation, and obtained up to second order the solutions for the compressible Poiseuille flow in both tubes and channels. The solution of the latter problem was also derived by Venerus and Bugajsky (2010) using the stream function/vorticity formulation.

All the above studies concerned only Newtonian flows. Viscoelasticity was taken into account only very recently by Housiadas and Georgiou (2011) who considered the plane Poiseuille flow of an Oldroyd-B fluid and extended the primary-variable perturbation scheme of Taliadorou et al. (2009a). The viscoelastic extra-stress tensor was an extra-field that was perturbed. In the present work, we derive the second-order regular perturbation solution of the axisymmetric Poiseuille flow of a liquid following the Oldroyd-B model. The limitations of this model are well known; however, we need to stress here that it is not possible

to obtain analytical solutions with other, more realistic, constitutive equations, like the Phan-Thien and Tanner and Giesekus models.

Along with the analytical solution, we also offer the resulting expressions for the average viscometric properties of the fluid, the pressure drop, the volumetric flow rate, and the difference of the total stress in the main flow direction between the exit and the entrance of the tube. Most importantly, the skin friction factor is also derived and discussed, extending thus the Newtonian results of Venerus (2006).

The rest of the paper is organized as follows. In "Governing equations", the conservation equations, the constitutive model, and the equation of state are presented in both dimensional and dimensionless forms. The perturbation procedure is described in "Perturbation solution" and the analytical solution up to second order in terms of the compressibility parameter presented. In "Results and discussion", criteria for the validity of the perturbation solution are provided and important features of the solution are underlined. The main conclusions of this work are summarized in the last section.

Governing equations

We consider the isothermal, steady, pressure-driven flow of a weakly compressible viscoelastic fluid in a circular tube with constant radius R^* and length L^*; note that throughout the extra-star denotes a dimensional quantity. Cylindrical coordinates is the natural choice for describing the flow. For isothermal, steady flow, and neglecting gravity, the continuity and momentum equations are:

$$\underline{\nabla}^* \cdot \left(\rho^* \underline{u}^*\right) = 0 \tag{1}$$

$$\rho^* \underline{u}^* \cdot \underline{\nabla}^* \underline{u}^* = \underline{\nabla}^* \cdot \underline{\underline{T}}^* \tag{2}$$

where ρ^* is the mass density of the fluid, $\underline{u}^*$ is the velocity vector, and $\underline{\underline{T}}^*$ is the total stress tensor:

$$\underline{\underline{T}}^* = -p^* \underline{\underline{I}} + \eta_s^* \underline{\underline{\dot{\gamma}}}^* + \underline{\underline{\tau}}^* \tag{3}$$

In Eq. 3, p^* is the total pressure, η_s^* is the constant zero shear-rate (Newtonian) viscosity of the pure solvent, $\underline{\underline{\dot{\gamma}}}^*$ is the augmented shear-rate tensor, $\underline{\underline{\tau}}^*$ is the additional extra-stress tensor introduced due to the presence of the polymer, and $\underline{\underline{I}}$ is the unit tensor. For a compressible fluid with zero bulk viscosity, the augmented rate-of-strain tensor, $\underline{\underline{\dot{\gamma}}}^*$, is defined as:

$$\underline{\underline{\dot{\gamma}}}^* = \underline{\nabla}^* \underline{u}^* + \left(\underline{\nabla}^* \underline{u}^*\right)^T - \frac{2}{3}\left(\underline{\nabla}^* \cdot \underline{u}^*\right) \underline{\underline{I}} \tag{4}$$

where the superscript T denotes the transpose of a tensor. A constitutive equation relating the extra-stress tensor to the shear-rate tensor is required for the closure of the system (1–4). In this study, we employ the Oldroyd-B constitutive model, given by the following equation:

$$\underline{\underline{\tau}}^* + \lambda^* \left[\frac{\partial \underline{\underline{\tau}}^*}{\partial t^*} + \underline{u}^* \cdot \underline{\nabla}^* \underline{\underline{\tau}}^* - \underline{\underline{\tau}}^* \cdot \underline{\nabla}^* \underline{u}^* - \left(\underline{\nabla}^* \underline{u}^*\right)^T \cdot \underline{\underline{\tau}}^* \right] = \eta_p^* \underline{\underline{\dot{\gamma}}}^* \tag{5}$$

where η_p^* and λ^* are, respectively, the zero shear-rate viscosity and the single relaxation time of the polymer. The mass density of the fluid is assumed to follow a linear equation of state:

$$\rho^* = \rho_0^* \left[1 + \varepsilon^* \left(p^* - p_0^*\right)\right] \tag{6}$$

where ρ_0^* is the mass density at a reference pressure p_0^*, $\varepsilon^* = -\left(\partial V / \partial P^*\right)_{P_0^*, T_0^*} / V_0^*$ is the isothermal compressibility coefficient, which is a assumed to be constant, V^* is the specific volume, and V_0^* is the specific volume at the reference pressure, p_0^*, and temperature, T_0^*. The value of ε^* is of the order of 0.001 MPa^{-1} for molten polymers (Hatzikiriakos and Dealy 1994) and increases by an order of magnitude (0.0178–0.0247 MPa^{-1}) in the case of PTFE pastes (Mitsoulis and Hatzikiriakos 2009). The latter authors suggest that for weakly compressible flows, ε^* ranges between 0 and 0.02 MPa^{-1} (for slightly to moderately compressible materials).

The boundary conditions for this Poiseuille flow are the usual ones. Along the wall no-slip and no-penetration are assumed and along the axis symmetry conditions are imposed. Moreover, the pressure is taken as zero at a point of the exit plane ($r^* = R^*$, $z^* = L^*$), and the mass flow-rate is specified at the exit of the tube ($z^* = L^*$):

$$u_z^*(R^*, z^*) = u_r^*(R^*, z^*) = 0, \quad 0 \le z^* \le L^* \tag{7}$$

$$\frac{\partial u_z^*}{\partial r^*}(0, z^*) = u_r^*(0, z^*) = 0, \quad 0 \le z^* \le L^* \tag{8}$$

$$p^*(R^*, L^*) = 0 \tag{9}$$

$$2\pi \int_0^{R*} \rho^* u_z^* r^* \, dr^* = \dot{M}^* \quad \text{at } z^* = L^* \tag{10}$$

where $\dot{M}^*$ is the constant mass flow-rate. No boundary conditions are specified at the inlet plane ($z^* = 0$), as

discussed by Poinsot and Lele (1992), Venerus (2006), and Housiadas and Georgiou (2011).

Dimensionless governing equations and auxiliary conditions

Equations 1–6 and the auxiliary conditions (7–10) are made dimensionless by using the characteristic scales reported in Table 1, where the characteristic velocity U^* is defined as the mean velocity at the exit of the tube:

$$U^* \equiv \dot{M}^* / \left(\pi \rho_0^* R^{*2}\right) \tag{11}$$

The pressure scale is such that the dimensionless pressure gradient in incompressible flow is equal to unity.

The dimensionless forms of the continuity equation, the components of the momentum equation, the non-trivial components of the constitutive model, and the equation of state, respectively, are:

$$\frac{\partial(\rho r u_r)}{\partial r} + \frac{\partial(\rho r u_z)}{\partial z} = 0 \tag{12}$$

$$\begin{aligned} &\widehat{Re}\rho\left(u_r\frac{\partial u_z}{\partial r} + u_z\frac{\partial u_z}{\partial z}\right) \\ &\quad = -8\frac{\partial p}{\partial z} + \eta_s\left\{a^2\frac{\partial^2 u_z}{\partial z^2} + \frac{\partial^2 u_z}{\partial r^2} + \frac{1}{r}\frac{\partial u_z}{\partial r}\right. \\ &\qquad\qquad \left. + \frac{a^2}{3}\left(\frac{\partial^2 u_z}{\partial z^2} + \frac{\partial^2 u_r}{\partial r \partial z} + \frac{1}{r}\frac{\partial u_r}{\partial z}\right)\right\} \\ &\qquad + \eta_p\left\{a^2\frac{\partial \tau_{zz}}{\partial z} + a\left(\frac{\partial \tau_{rz}}{\partial r} + \frac{\tau_{rz}}{r}\right)\right\} \end{aligned} \tag{13}$$

$$\begin{aligned} &a^2\widehat{Re}\rho\left(u_r\frac{\partial u_r}{\partial r} + u_z\frac{\partial u_r}{\partial z}\right) \\ &\quad = -8\frac{\partial p}{\partial r} + \eta_s a^2\left\{a^2\frac{\partial^2 u_r}{\partial z^2} + \frac{\partial^2 u_r}{\partial r^2} + \frac{1}{r}\frac{\partial u_r}{\partial r} - \frac{u_r}{r^2}\right. \\ &\qquad\qquad \left. + \frac{1}{3}\left(\frac{\partial^2 u_z}{\partial z \partial r} + \frac{\partial^2 u_r}{\partial r^2} + \frac{1}{r}\frac{\partial u_r}{\partial r} - \frac{u_r}{r^2}\right)\right\} \\ &\qquad + \eta_p a^2\left\{a\frac{\partial \tau_{rz}}{\partial z} + \frac{\partial \tau_{rr}}{\partial r} + \frac{\tau_{rr} - \tau_{\theta\theta}}{r}\right\} \end{aligned} \tag{14}$$

$$\begin{aligned} &\tau_{zz} + We\left(u_r\frac{\partial \tau_{zz}}{\partial r} + u_z\frac{\partial \tau_{zz}}{\partial z} - 2\tau_{zz}\frac{\partial u_z}{\partial z} - \frac{2\tau_{rz}}{a}\frac{\partial u_z}{\partial r}\right) \\ &\quad = \frac{4}{3}\frac{\partial u_z}{\partial z} - \frac{2}{3}\left(\frac{\partial u_r}{\partial r} + \frac{u_r}{r}\right) \end{aligned} \tag{15}$$

$$\begin{aligned} &\tau_{rz} + We\left(u_r\frac{\partial \tau_{rz}}{\partial r} + u_z\frac{\partial \tau_{rz}}{\partial z} - \tau_{rz}\left(\frac{\partial u_z}{\partial z} + \frac{\partial u_r}{\partial r}\right)\right. \\ &\qquad \left. - \tau_{zz}a\frac{\partial u_r}{\partial z} - \frac{\tau_{rr}}{a}\frac{\partial u_z}{\partial r}\right) = a\frac{\partial u_r}{\partial z} + \frac{1}{a}\frac{\partial u_z}{\partial r} \end{aligned} \tag{16}$$

$$\begin{aligned} &\tau_{rr} + We\left(u_r\frac{\partial \tau_{rr}}{\partial r} + u_z\frac{\partial \tau_{rr}}{\partial z} - 2\tau_{rr}\frac{\partial u_r}{\partial r} - 2a\tau_{rz}\frac{\partial u_r}{\partial z}\right) \\ &\quad = \frac{4}{3}\frac{\partial u_r}{\partial r} - \frac{2}{3}\left(\frac{\partial u_z}{\partial z} + \frac{u_r}{r}\right) \end{aligned} \tag{17}$$

$$\begin{aligned} &\tau_{\theta\theta} + We\left(u_r\frac{\partial \tau_{\theta\theta}}{\partial r} + u_z\frac{\partial \tau_{\theta\theta}}{\partial z} - 2\frac{u_r\tau_{\theta\theta}}{r}\right) \\ &\quad = \frac{4}{3}\frac{u_r}{r} - \frac{2}{3}\left(\frac{\partial u_r}{\partial r} + \frac{\partial u_z}{\partial z}\right) \end{aligned} \tag{18}$$

$$\rho = 1 + \varepsilon p \tag{19}$$

and the domain of definition is $\{0 \le r \le 1, 0 \le z \le 1\}$. In Eqs. 12–19 there appear six dimensionless numbers: the Reynolds and Weissenberg numbers, Re and We, the dimensionless compressibility parameter, ε, the tube aspect ratio, α, and the viscosity ratios, η_s and η_p. For convenience, all definitions are tabulated in Table 2. In Eqs. 13 and 14, the modified Reynolds number $\widehat{Re} \equiv aRe$ has been employed. With the chosen scales, $\eta_s + \eta_p = 1$ and the dimensionless total stress tensor is $\underline{\underline{T}} = -8p\underline{\underline{I}}/a^2 + \eta_s\dot{\underline{\underline{\gamma}}} + \eta_p\underline{\underline{\tau}}$. The Mach number for this flow is defined as $Ma \equiv \sqrt{\varepsilon Re/\left(8c_p^*/c_v^*\right)}$, where c_p^*/c_v^* is the heat capacity ratio. In the present work, only subsonic flows are considered, such that $Ma << 1$. The dimensionless boundary and auxiliary conditions are:

$$u_z(1, z) = u_r(1, z) = 0, \quad 0 \le z \le 1 \tag{20}$$

Table 1 Characteristic scales

Axial distance, z^*	Radial distance, r^*	Axial velocity, u_z^*	Radial velocity, u_r^*	Shear rate, $\dot{\gamma}_{ij}^*$	Pressure, $p*$	Mass density, ρ^*	Viscoelastic extra-stress, $\underline{\underline{\tau}}^*$
L^*	R^*	U^*	$\frac{U^*R^*}{L^*}$	$\frac{U^*}{L^*}$	$\frac{8\left(\eta_s^* + \eta_p^*\right)L^*U^*}{R^{*2}}$	ρ_0^*	$\frac{\eta_p^*U^*}{L^*}$

Table 2 Dimensionless number and parameters appearing in Eqs. 13–19

Reynolds number, Re	Modified Reynolds number, $\widehat{Re}$	Aspect ratio, a	Weissenberg number, We	Compressibility parameter, ε	Solvent viscosity ratio, η_s	Polymer viscosity ratio, η_p
$\frac{\rho_0^* U^* R^*}{\eta_s^* + \eta_p^*}$	$\frac{\rho_0^* U^* R^{*2}}{\left(\eta_s^* + \eta_p^*\right) L^*}$	$\frac{R^*}{L^*}$	$\frac{\lambda^* U^*}{L^*}$	$\frac{8\left(\eta_s^* + \eta_p^*\right)\varepsilon^* L^* U^*}{R^{*2}}$	$\frac{\eta_s^*}{\eta_s^* + \eta_p^*}$	$\frac{\eta_p^*}{\eta_s^* + \eta_p^*}$

$$\frac{\partial u_z}{\partial r}(0, z) = u_r(0, z) = 0, \quad 0 \le z \le 1 \tag{21}$$

$$p(1, 1) = 0 \tag{22}$$

$$2\int_0^1 \rho u_z r dr = 1 \quad \text{at} \quad z = 1 \tag{23}$$

Perturbation solution

A regular perturbation scheme in terms of the compressibility parameter, ε, is employed:

$$X = X_0 + \varepsilon X_1 + \varepsilon^2 X_2 + O(\varepsilon^3) \tag{24}$$

where X is a primary variable of the flow, i.e., one of ρ, p, u_r, u_z, τ_{rr}, τ_{rz}, τ_{zz}, $\tau_{\theta\theta}$. Note that $\rho_0 = 1$ as suggested explicitly by Eq. 19. We also assume that $u_{r0} = 0$ and $u_{r1} = 0$ in order to be able to derive a separable solution. The same perturbation scheme and assumptions were used by Taliadorou et al. (2009a) and Housiadas and Georgiou (2011).

Substituting the expansions (24) into the governing equations and collecting terms of the same order, lead to a sequence of partial differential equations and accompanying boundary conditions. The zero-, first-, and second-order problems are solved analytically by following a similar procedure like the one described in our recent article for the planar case (Housiadas and Georgiou 2011). The details can be found in Mamoutos (2010).

Because some expressions are very long, we use, for convenience, the superscripts (N) and (V) to denote respectively the Newtonian and viscoelastic parts of a primary variable X, i.e.

$$X \equiv X^{(N)} + X^{(V)}$$

For the different terms of the viscoelastic parts, we also use the following notation:

$$X^{(V)} \equiv X^{(V,0)} + \varepsilon X^{(V,1)} + \varepsilon^2 X^{(V,2)}$$

Pressure

$$\begin{aligned} p^{(N)} = {} & (1 - z) \\ & + \varepsilon \left\{ \frac{a^2}{12}\left(1 - r^2\right) + \frac{\widehat{Re}}{4}(1 - z) - \frac{1}{2}(1 - z)^2 \right\} \\ & + \varepsilon^2 \left\{ \frac{a^2 \widehat{Re}}{432}\left(-10r^6 + 45r^4 - 54r^2 + 19\right) + (1 - z) \right. \\ & \times \left[\frac{a^2}{108}\left(27r^2 - 87\right) + \frac{\widehat{Re}^2}{27} - \frac{\widehat{Re}}{2}(1 - z) \right. \\ & \left. \left. + \frac{1}{2}(1 - z)^2 \right] \right\} \end{aligned} \tag{25a}$$

$$\begin{aligned} p^{(V)} = {} & \varepsilon \eta_p We \left\{ -\frac{28}{9}(1 - z) + \frac{\varepsilon}{27}\left[a^2\left(33r^4 - 43r^2 + 10\right) \right. \right. \\ & - \frac{369}{10}\widehat{Re}(1 - z) + 2(z - 1) \\ & \left. \left. \times \left(8We\left(12 + 25\eta_p\right) + 105(1 - z)\right) \right] \right\} \end{aligned} \tag{25b}$$

Velocity components

$$\begin{aligned} u_z^{(N)} = {} & 2\left(1 - r^2\right) \left[1 + \varepsilon \left\{ \frac{\widehat{Re}}{18}\left(-r^4 + \frac{7}{2}r^2 - 1 \right) - (1 - z) \right\} \right. \\ & + \frac{\varepsilon^2}{2}\left\{ 3(1 - z)^2 + \frac{a^2}{8}\left(\frac{1}{9} - 3r^2 \right) \right. \\ & \times \frac{\widehat{Re}}{6}(1 - z)\left(2r^4 - 7r^2 - 1\right) \\ & + \frac{\widehat{Re}^2}{21,600}\left(43 - 957r^2 + 2,343r^4 \right. \\ & \left. \left. \left. -1,257r^6 + 168r^8\right) \right\} \right] \end{aligned} \tag{26a}$$

$$u_z^{(V,0)} = 0$$

$$u_z^{(V,1)} = -\frac{8}{9}\eta_p We\left(3r^4 - 4r^2 + 1\right)$$

$$u_z^{(V,2)} = \eta_p We\left\{\frac{8We}{27}\left(-13 + 60r^2 - 63r^4 + 16r^2 - 2\eta_p\left(3 - 10r^2 + 3r^4 + 4r^6\right)\right) + \frac{8}{9}(1-z)\left(11 - 23r^2 + 12r^4\right) + \frac{\widehat{Re}}{270}\left(-13 - 122r^2 + 540r^4 - 500r^6 + 95r^8\right)\right\} \quad (26b)$$

$$u_r^{(N)} = \frac{1}{36}\varepsilon^2\widehat{Re}r\left(4 - r^2\right)\left(1 - r^2\right)^2 \quad (27a)$$

$$u_r^{(V)} = \frac{4}{3}\varepsilon^2\eta_p Wer\left(1 - r^2\right)^2 \quad (27b)$$

Extra-stress components

$$\tau_{zz}^{(N)} = \varepsilon\left(1 - r^2\right)\left[\frac{8}{3} + \varepsilon\left\{\frac{2}{27}\,\widehat{Re}\left(-8r^4 + 28r^2 + 1\right) - 8(1-z)\right\}\right] \quad (28a)$$

$$\tau_{zz}^{(V,0)} = 32We\left(\frac{r}{a}\right)^2 \quad (28b)$$

$$\tau_{zz}^{(V,1)} = 256We\left(\frac{r}{a}\right)^2\left\{\frac{\widehat{Re}}{3}\left(-2r^4 + 6r^2 - 3\right) - \frac{8}{3}We\left(1 - r^2 + \frac{4}{3}\eta_p\left(2 - 3r^2\right)\right) - 4(1-z)\right\} \quad (28c)$$

$$\tau_{zz}^{(V,2)} = We\left\{-\frac{8}{9}\left(6 - 26r^2 + 33r^4\right) - \frac{16}{27}\eta_p\left(25 - 58r^2 + 33r^4\right) + \left(\frac{r}{a}\right)^2\left[\frac{2\widehat{Re}}{135}\left(235 - 1{,}200r^2 + 1{,}800r^4 - 930r^6 + 144r^8\right) + 128(1-z)^2 + \frac{128}{3}We(1-z) \times \left(5\left(1 - r^2\right) + 2\eta_p\left(9 - 10r^2\right)\right) + We^2\left(3\left(1 - r^2\right)^2 + \frac{4\eta_p^2}{81} \times \left(36r^4 - 15r^2 - 7\right) + \frac{\eta_p}{27}\left(117r^4 - 152r^2 + 53\right)\right) + \widehat{Re}\left[We\left\{\frac{16}{27}\left(148 - 513r^2 + 492r^2 - 127r^6\right) + \frac{32\eta_p}{135}\left(181 - 960r^2 + 1{,}190r^4 - 310r^6\right)\right\} + \frac{16}{3}\left(9 - 24r^2 + 8r^4\right)(1-z)\right]\right]\right\} \quad (28d)$$

$$\tau_{rz}^{(N)} = \frac{r}{a}\left\{-4 + \varepsilon\left[\widehat{Re}\left(1 - 2r^2 + \frac{2}{3}r^4\right) + 4(1-z) + \varepsilon\left\{-\frac{\widehat{Re}^2}{540}\left(50 - 330r^2 + 540r^4 - 285r^6 + 42r^8\right) - 2\widehat{Re}(1-z)\left(r^2 - r - 1\right)\left(r^2 + r - 1\right) + \frac{a^2\left(-14 + 27r^2\right)}{18} - 6(1-z)^2\right\}\right]\right\} \quad (29a)$$

$$\tau_{rz}^{(V,0)} = 0 \quad (29b)$$

$$\tau_{rz}^{(V,1)} = \frac{16r}{9a}We\left(3\left(1 - r^2\right) + 2\eta_p\left(2 - 3r^2\right)\right) \quad (29c)$$

$$\tau_{rz}^{(V,2)} = \frac{We}{a} r \left\{ \frac{16\,(1-z)}{3} \left[\eta_p \frac{24r^2-23}{3} - 4\left(1-r^2\right) \right] - 32We \left[2\left(1-r^2\right)^2 + \frac{2\eta_p^2}{27}\left(-5+3r^2+6r^4\right) + \frac{\eta_p\left(10-35r^2+28r^4\right)}{9} \right] + \frac{2\widehat{Re}}{27} \left[-2\left(1-r^2\right)\left(29-106r^2+35r^4\right) + \frac{\eta_p}{5}\left(-61+540r^2-750r^4+190r^6\right) \right] \right\} \tag{29d}$$

$$\tau_{rr}^{(N)} = \varepsilon\left(1-r^2\right)\left\{ -\frac{4}{3} + \varepsilon\left(\frac{\widehat{Re}}{54}\left(25r^4-83r^2-2\right) + 4\,(1-z) \right) \right\} \tag{30a}$$

$$\tau_{rr}^{(V)} = \frac{8}{27}\varepsilon^2 We\left(1-r^2\right)\left(\eta_p\left(25-51r^2\right)+27\left(1-r^2\right)\right) \tag{30b}$$

$$\tau_{\theta\theta}^{(N)} = \varepsilon\left(1-r^2\right)\left\{ -\frac{4}{3} + \varepsilon\left(\frac{\widehat{Re}}{54}\left(7r^4-29r^2-2\right) + 4\,(1-z) \right) \right\} \tag{31a}$$

$$\tau_{\theta\theta}^{(V)} = \frac{8}{27}\varepsilon^2 We\left(1-r^2\right)\left(\eta_p\left(25-15r^2\right)+27\left(1-r^2\right)\right) \tag{31b}$$

Results and discussion

In this section, we first provide some criteria for the validity of the perturbation solution derived in the previous section. We also calculate cross-sectional average profiles and other useful quantities, such as the pressure drop, the difference at the total axial stress between the exit and the entrance of the tube, and the skin friction factor. It is readily verified that the Newtonian parts of the perturbation solution are the same as those obtained for the Newtonian flow (i.e., for $We = 0$) by Taliadorou et al. (2009b) and subsequently by Venerus and Bugajsky (2010).

Unless otherwise indicated, in all the results presented in this section the aspect ratio is taken to be $\alpha = 0.1$ and the polymer viscosity $\eta p = 8/9$ (which implies that $\eta s = 1/9$).

Validity of the perturbation scheme

We start by considering the mass density of the fluid at the exit of the tube ($z = 1$) for which Eqs. 19 and 25a, b give:

$$\rho\,(r,1) = 1 + \frac{a^2\varepsilon^2}{12}\left(1-r^2\right) \times \left\{ 1 + \frac{\varepsilon\widehat{Re}}{36}\left(19-35r^2+10r^4\right) + \frac{4}{9}\varepsilon\eta_p We\left(10-33r^2\right) \right\} + O\left(\varepsilon^4\right) \tag{32}$$

The above result shows that at first order there is no effect of the fluid compressibility, fluid inertia, and viscoelasticity on the density at the tube exit. Since only very small variations of the density are acceptable (the fluid is decompressed and the mass density reaches its lowest values at $r = z = 1$), it follows that there must be $\varepsilon^2 a^2/12 << 1$.

For the dimensionless volumetric flow rate, we get:

$$Q\,(z) = 1 - \varepsilon\,(1-z) + \varepsilon^2\left[-\frac{a^2}{18} + \frac{3}{2}\,(1-z)^2 + (1-z) \times \left(\frac{28}{9}\eta_p We - \frac{1}{4}\widehat{Re} \right) \right] + O\left(\varepsilon^3\right) \tag{33}$$

At the inlet plane ($z = 0$), we have

$$Q\,(0) \approx 1 - \varepsilon + c\varepsilon^2 \tag{34}$$

where

$$c = \frac{3}{2} - \frac{a^2}{18} - \frac{1}{4}\widehat{Re} + \frac{28}{9}We\eta_p \tag{35}$$

Hence, $Q\,(0)$ is a parabola with the minimum at $\varepsilon_c = 1/(2c)$. However, any increase of ε must lead to more compression, i.e., to a lower value for $Q(0)$, and therefore the perturbation solution is valid only when $0 \le \varepsilon \le \varepsilon_c$. It is also clear that if ε is specified, critical values can be obtained for the constant c or the Reynolds number $\widehat{Re}$ or the quantity $\eta_p We$ by solving the latter inequality.

From Eq. 35 it is also deduced that viscoelasticity reduces the upper limit of validity of the perturbation scheme and that increasing the Reynolds number or the aspect ratio has the opposite effect. A similar observation holds for the flow in a slit (Housiadas and

Georgiou 2011). Figure 1a shows the volumetric flow rates at the entrance of the tube as a function of the compressibility parameter, ε, for different Weissenberg numbers ($We = 0$, 0.2, and 0.4) at a modified Reynolds number $\widehat{Re} = 1$ and an aspect ratio $a = 0.1$, while Fig. 1b shows $Q(0)$ as a function of ε for $\widehat{Re} = 0.1$, 1.0, 3.0 at a Weissenberg number $We = 0.2$ and $a = 0.1$.

From Eq. 35 the maximum acceptable modified Reynolds number, $\widehat{Re}$, can be obtained demanding that $c > 0$ which yields:

$$\widehat{Re} < 6 - \frac{2}{9}a^2 + \frac{112}{9}\eta_p We \tag{36}$$

Therefore, the maximum allowed modified Reynolds number is about 6 for a Newtonian fluid, while for a viscoelastic fluid is larger and depends on the quantity $\eta_p We$.

Average quantities

The cross-sectional average of a (dimensionless) variable $f = f(r,z)$ is calculated by means $\langle f \rangle = 2\int_0^1 rf\,dr$. Thus, for the radial velocity component and the pressure, we find:

$$\langle u_r \rangle = \frac{4}{5}\varepsilon^2\left(\frac{11\widehat{Re}}{567} + \frac{16}{65}\eta_p We\right) + O\left(\varepsilon^3\right) \tag{37}$$

$$\begin{aligned}\langle p \rangle = {} & (1-z) + \varepsilon\left[\frac{a^2}{24} - \frac{1}{2}(1-z)^2 + \left(\frac{1}{4}\widehat{Re} - \frac{28}{9}\eta_p We\right)(1-z)\right] \\ & + \varepsilon^2\left[\begin{array}{l}\frac{1}{2}(1-z)^3 - \frac{49}{72}a^2(1-z) + \widehat{Re}\left\{\frac{a^2}{96} + \left(\frac{1}{27}\widehat{Re} - \frac{41}{30}\eta_p We\,(1-z) - \frac{1}{2}(1-z)\right)(1-z)\right\} \\ + \eta_p We\left\{-\frac{a^2}{45} + \frac{16}{27}We\,(12+25\eta_p)(1-z) + \frac{70}{9}(1-z)^2\right\}\end{array}\right] + O\left(\varepsilon^3\right)\end{aligned} \tag{38}$$

It should be noted that the average axial velocity component is actually the same with the dimensionless volumetric flow rate, Q, given above, i.e., $\langle u_z \rangle = Q$. The average mass density of the fluid also follows the abovementioned expression for the pressure, since due to Eq. 19, $\langle \rho \rangle = 1 + \varepsilon \langle \rho \rangle$. In Fig. 2, we show the average mass density of the fluid as a function of the axial distance for a Newtonian ($We = 0$) and two viscoelastic fluids with $We = 0.2$ and 0.4. First, the decompression of the fluid under consideration is clearly seen in all cases. As thefluid goes through the tube is decompressed reaching to a fully decompressed state at the exit of the tube. Notice that the differences between different radial locations are undistinguishable, showing that the

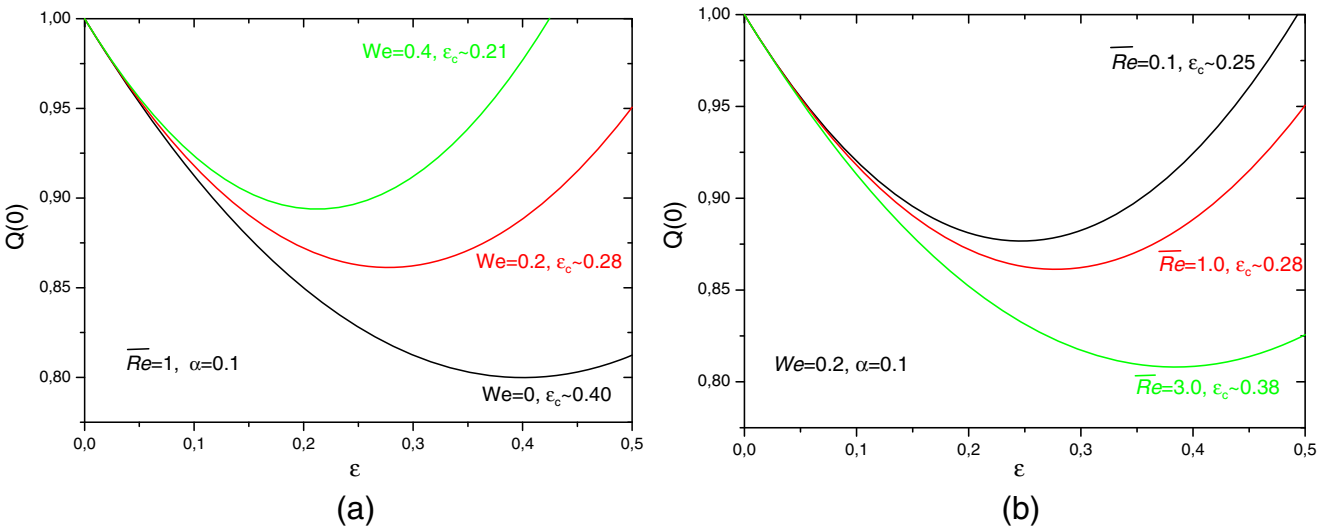

Fig. 1 The volumetric flow rate at the entrance of the tube as a function of the dimensionless compressibility parameter for: **a** $\widehat{Re} = 1$ and various values of We; **b** $We = 0.2$ and various modified Reynolds numbers

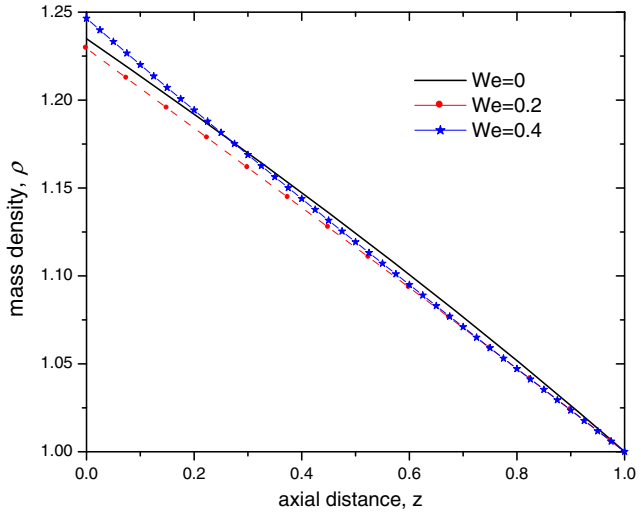

Fig. 2 The mass density of the fluid as a function of the axial coordinate, for a Newtonian fluid and two viscoelastic fluids with $We = 0.2$ and 0.4; $\varepsilon = 0.2$ and $\widehat{Re} = 1$

variations of the fluid density in the cross-section of the tube are negligible; thus the relation $\langle\rho\rangle = 1 + \varepsilon\,\langle p\rangle$, where $\langle p\rangle$ is given by Eq. 38, can be safely used at any radial distance from the center of the tube. Regarding the differences between the Newtonian and the viscoelastic fluid, it appears that these are small, and the trends depend on the magnitude of the Weissenberg number. In particular, for the low Weissenberg number 0.2, the fluid is slightly less compressed than the Newtonian one; however, the opposite holds for $We = 0.4$. Nevertheless, all of them are decompressed almost linearly with respect to the axial distance, z.

Cross-sectional averages have also been derived for the components of the dimensionless total stress tensor, $\underline{\underline{\hat{T}}} \equiv (a^2/8)\,\underline{\underline{T}}$. Here, we report only the results for the shear stress component, $\left\langle \hat{T}_{rz} \right\rangle$, and the first, $\left\langle \hat{N}_1 \right\rangle \equiv \left\langle \hat{T}_{zz} - \hat{T}_{rr} \right\rangle$, and second, $\left\langle \hat{N}_2 \right\rangle \equiv \left\langle \hat{T}_{zz} - \hat{T}_{\theta\theta} \right\rangle$, normal-stress differences. In particular, using the analytical expressions 26a–28d, we find:

$$\left\langle \hat{T}_{rz} \right\rangle = -\frac{a}{3} + \varepsilon a\left(\frac{1}{3}(1-z) + \frac{\widehat{Re}}{140} + \frac{32}{135}\eta_p We\right) + \varepsilon^2 a\left(\frac{11a^2}{1{,}080} + \frac{\widehat{Re}^2}{55{,}400} - \frac{8\eta_p We^2\,(345+148\eta_p)}{2{,}835} + \widehat{Re}\left(\frac{29\eta_p We}{630} + \frac{13\,(1-z)}{210}\right) - \frac{268}{135}\eta_p We\,(1-z) - \frac{(1-z)^2}{2}\right) + O\left(\varepsilon^3\right) \tag{39}$$

Equation 39 shows that the average shear stress at zero order is solely due to the viscous forces of the fluid, as it should, since at this order there is no effect of the fluid compressibility. However, at higher order we have combined effects of fluid compressibility with viscous, viscoelastic, and inertial forces. At first order, all contributions in the total shear stress are positive which clearly show that the combined effect of fluid compressibility with viscous, inertial, or viscoelastic forces cause a decrease of the drag force at the wall of the tube.

For the first normal difference we find:

$$\left\langle \hat{N}_1 \right\rangle = 2\eta_p We + \varepsilon\left[\frac{a^2}{4} - \frac{8}{9}\eta_p We^2 - 4\eta_p We\,(1-z)\right] + \varepsilon^2\left[\begin{array}{c} \frac{11}{1,080}\widehat{Re}^2\eta_p We + \frac{8}{81}\eta_p We^3 + \widehat{Re}\left[\frac{41a^2}{576} + \frac{2}{45}\eta_p\,(1+4\eta_p)\,We^2 - \eta_p We\,(1-z)\right] + \\ \eta_p We\left(8\,(1-z)^2 - \frac{13}{9}a^2\right) + \frac{8}{9}\eta_p We^2\,(5+14\eta_p)\,(1-z) - \frac{3}{4}a^2\,(1-z)^2 \end{array}\right] + O\left(\varepsilon^3\right) \tag{40}$$

Equation 40 shows that at first-order combined effects of compressibility with viscous and viscoelastic forces appear. Also, $\left\langle \hat{N}_1 \right\rangle$ is a linear function of the axial coordinate at first order and a quadratic one at second order. It is worth mentioning that even for a Newtonian fluid ($We = 0$ or $\eta_p = 0$) the average first normal stress difference is non-zero due to the combined effects of fluid compressibility with inertial and viscous forces.

Results for $\left\langle \hat{T}_{rz} \right\rangle$ and $\left\langle \hat{N}_1 \right\rangle$ as functions of the axial distance, z, are shown in Fig. 3, for three different fluids with $We = 0$, 0.2, and 0.4. In particular, in Fig. 3a the average total shear-stress is plotted. In all cases, it is observed that the shear-stress decreases monotonically reaching its minimum at the exit of tube. As the viscoelasticity of the fluid increases, the shear-rate near the entrance of the tube decreases. However, this trend

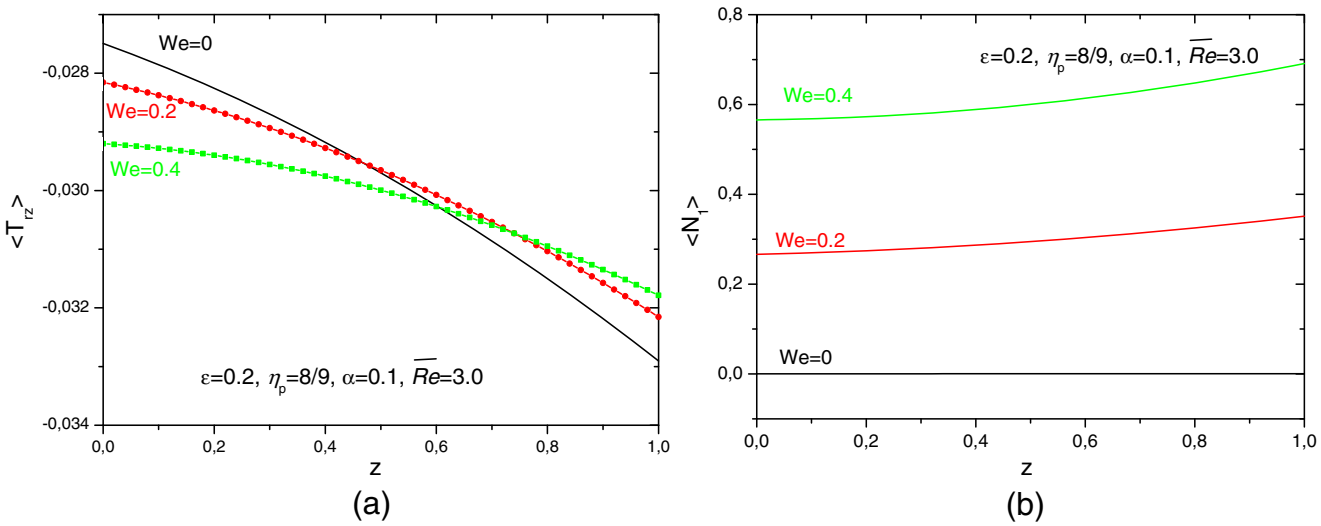

Fig. 3 Average quantities as functions of the dimensionless length **a** the total shear stress **b** the first normal stress difference. The parameters are the same as in Fig. 2

is reversed downstream, from the middle of the tube till the outflow plane. The magnitude of the average first normal stress difference is affected mainly by the polymer viscosity ratio and the Weissenberg number, as Eq. 40 shows, which is of course the case for an incompressible Oldroyd-B model. It varies quadratically with the axial distance, but this dependence is rather weak.

For the second normal stress difference the following expression is obtained:

$$\left\langle \hat{N}_2 \right\rangle = -\frac{\varepsilon^2 a^2}{9}\left(\frac{5\widehat{Re}}{32} + 2\eta_p We\right) + O\left(\varepsilon^3\right) \tag{41}$$

The combined compressibility/inertia and compressibility/viscoelastic effects give rise to negative second normal stress difference at first order, while for the incompressible Oldroyd-B fluid, $\left\langle \hat{N}_1 \right\rangle = 0$. As it is usually the case with viscoelastic fluids, the predicted second normal stress difference is much smaller than the corresponding first normal stress difference. Note also that $\left\langle \hat{N}_2 \right\rangle$ is constant throughout the length of the tube and that for a Newtonian fluid, i.e., for $We = 0$ or $\eta_p = 0$, i.e., a non-zero $\left\langle \hat{N}_2 \right\rangle$ arises due to the combined effect of fluid compressibility with inertia.

Pressure drop, friction factor, and flow curves

Let the symbol Δ denote the difference of a quantity ϕ between the exit and the entrance of the tube, i.e., $\Delta\phi \equiv \phi\,(z=1) - \phi\,(z=0)$. Then, the average pressure drop is given by:

$$\begin{aligned}\Delta\langle -p\rangle = {} & 1 - \varepsilon\left(\frac{1}{2} - \frac{1}{4}\widehat{Re}\right) \\ & + \varepsilon^2\left(\frac{1}{2} - \frac{49}{72}a^2 - \frac{1}{2}\widehat{Re} + \frac{1}{27}\widehat{Re}^2\right) \\ & + \varepsilon\eta_p We\left(-\frac{28}{9} + \varepsilon\left\{\frac{70}{9} - \frac{41}{30}\widehat{Re}\right.\right. \\ & \qquad \left.\left. + \frac{16We}{27}\left(25\eta_p + 12\right)\right\}\right) \\ & + O\left(\varepsilon^3\right)\end{aligned} \tag{42}$$

which is simply a generalization of the dimensionless Hagen-Poiseuille formula, taking into account the fluid compressibility combined with inertial, viscous, and viscoelastic forces. For an incompressible fluid Eq. 42 reduces to $\Delta\langle -p\rangle = 1$.

For the difference in the total axial stress in the main flow direction, we find a similar expression:

$$\begin{aligned}\Delta\left\langle \hat{T}_{zz}\right\rangle = {} & 1 - \varepsilon\left(\frac{1}{2} - \frac{1}{4}\widehat{Re}\right) \\ & + \varepsilon^2\left(\frac{1}{2} - \frac{13}{72}a^2 - \frac{1}{2}\widehat{Re} + \frac{1}{27}\widehat{Re}^2\right) \\ & + \varepsilon\eta_p We\left(-\frac{28}{9} + \varepsilon\left\{\frac{70}{9} - \frac{41}{30}\widehat{Re}\right.\right. \\ & \qquad \left.\left. + \frac{16We}{27}\left(25\eta_p + 12\right)\right\}\right) \\ & + O\left(\varepsilon^3\right)\end{aligned} \tag{43}$$

For $We = 0$ or $\eta_p = 0$, Eq. 43 reduces to the result of Venerus (2006) and Taliadorou et al. (2009a) for a compressible Newtonian fluid with zero bulk viscosity.

In Fig. 4, dimensionless flow curves are shown, i.e., curves of the volumetric flow rate at the entrance of the tube versus the pressure drop, constructed by varying the compressibility number ε from $\varepsilon = 0$ to $\varepsilon = \varepsilon_c$ (the upper limit of validity of the perturbation solution) and calculating $Q(0)$ and $\Delta\langle -p\rangle$ from Eqs. 33 and 42, respectively. For the Newtonian fluid ($We = 0$) and the weakly viscoelastic fluid ($We = 0.05$ and 0.1) it is seen that the flow curves are monotonic. However, as the Weissenberg number increases ($We = 0.2$ and 0.3) there is a range of $\Delta\langle -p\rangle$ for which two solutions for $Q(0)$p are admissible. It is also seen that for a given flow rate at the entrance of the tube, the lowest pressure drop is observed for the Newtonian fluid; the increase of the Weissenberg number increases the pressure drop. The same observations were also made for the flow in channel (Housiadas and Georgiou 2011).

Another interesting quantity is the friction factor, which actually represents a dimensionless shear stress at the wall. In particular, the Fanning friction factor, C_f, is defined as:

$$C_f \equiv \frac{T_w^*}{\frac{1}{2}\rho_0^* U^{*2}} \tag{44}$$

where

$$T_w^* = -\left(\eta_s^* \frac{\partial u_z^*}{\partial r^*} + \tau_{rz}^*\right)_{r=R^*} \tag{45}$$

is the total shear stress exerted by the fluid to the wall of the tube. The Darcy friction factor, $f = 4C_f$, is often used in the literature. Using the characteristic scales reported in Table 1, the dimensionless Darcy friction factor is given by:

$$f(z) = -\frac{8}{Re}\left(\eta_s \frac{\partial u_z}{\partial r}(1, z) + a\eta_p \tau_{rz}(1, z)\right) \tag{46}$$

Equation 46 shows that f is a function of the axial coordinate. Thus, we define an average Darcy friction factor, $\overline{f}$, along the entire tube which results from the integration of Eq. 46 from the entrance of the tube ($z = 0$) to its exit ($z = 1$). In addition, if we use expressions 26 and 29, we finally find:

$$\begin{aligned}\frac{Re}{32}\overline{f} = 1 &- \varepsilon\left(\frac{1}{2} - \frac{1}{12}\widehat{Re}\right) \\ &+ \varepsilon^2\left(\frac{1}{2} - \frac{13}{72}a^2 - \frac{1}{4}\widehat{Re} + \frac{17}{2,160}\widehat{Re}^2\right) \\ &+ \varepsilon\frac{8}{9}\eta_p We\left(1 + \varepsilon\left\{-\frac{1}{4} + \frac{27}{80}\widehat{Re}\right.\right. \\ &\qquad \left.\left. + We\left(\frac{8}{3}\eta_p + 3\right)\right\}\right) \\ &+ O\left(\varepsilon^3\right)\end{aligned} \tag{47}$$

Equation 47 can be useful in comparisons with experimental data. For $We = 0$ or $\eta_p = 0$ it reduces to the corresponding equation of Venerus (2006) for a Newtonian fluid. In Fig. 5, the quantity $Re\overline{f}/32$ is plotted as a function of $\widehat{Re}$ for a very compressible fluid with $\varepsilon = 0.2$ and various values of the Weissenberg number ($We = 0$, 0.1, 0.2). It is seen that the increase of the viscoelasticity in the flow increases both the skin friction factor and the magnitude of the pressure drop.

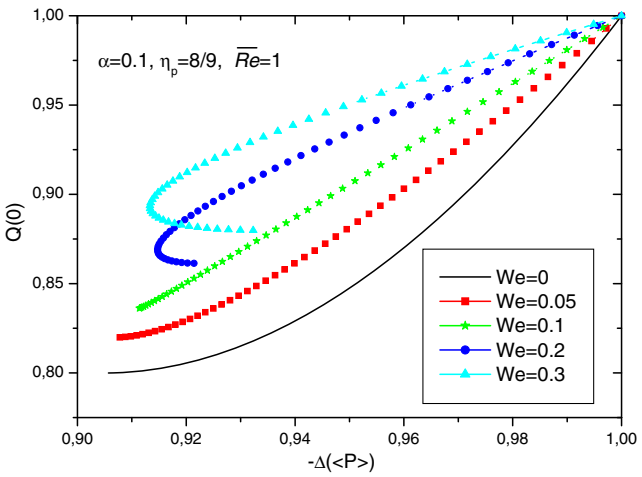

Fig. 4 The volumetric flow rate at the entrance of the tube as a function of the pressure drop for various Weissenberg numbers; $\varepsilon = 0.2$ and $\widehat{Re} = 1$

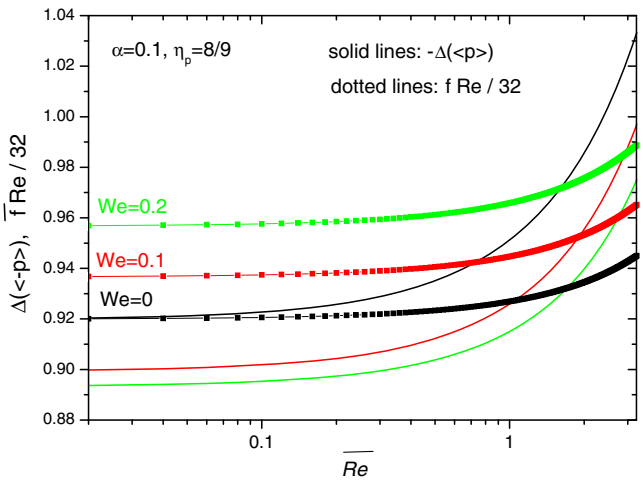

Fig. 5 The pressure drop and the average Darcy friction factor for different Weissenberg numbers as functions of the modified Reynolds number; $\varepsilon = 0.2$

It should be pointed out, however, that the values for the Weissenberg number are in the range for which only one solution in the flow-rate curve exists (see Fig. 4).

Expression 47 can also be derived with the aid of the momentum balance in the streamwise direction, Eq. 13, and the continuity equation, Eq. 12. In particular, multiplying Eq. 13 by $2r$, integrating with respect to r, simplifying the result, and using the definition of the Darcy friction factor, Eq. 46, we get an ordinary differential equation which by integration with respect to z, from $z = 0$ to $z = 1$, gives:

$$\frac{Re}{32}\overline{f} = \Delta\left(\left\langle \hat{T}_{zz}\right\rangle - \frac{\widehat{Re}}{8}\left\langle \rho u_z^2\right\rangle + \frac{a^2\eta_s}{12}\int_0^1 u_r dr\right) \tag{48}$$

where

$$\left\langle \hat{T}_{zz}\right\rangle = -\left\langle p\right\rangle + \frac{a^2}{8}\left(\frac{4\eta_s}{3}\frac{d\left\langle u_z\right\rangle}{dz} + \eta_p\left\langle \tau_{zz}\right\rangle\right). \tag{49}$$

It is emphasized that Eq. 48 is exact, i.e., no approximation or assumptions have been made for its derivation. It is actually a relation between the skin friction factor and the pressure drop. Venerus (2006) neglected the viscous term in the above expression. Nevertheless, although in the Newtonian case, $Re\overline{f}/32$, and $\Delta\left\langle \hat{T}_{zz}\right\rangle$ as given by Eqs. 48 and 43, respectively, are very similar, the terms due to the combined effect of compressibility and viscoelasticity are different and thus, Eq. 48 is to be preferred instead of Venerus approximation for the friction factor.

From the experimental point of view, it is not convenient to use Eqs. 42, 43, and 48 for the pressure drop, total axial stress, and skin friction factor, respectively, since both the compressibility parameter, ε, and the Weissenberg number, We, are defined with the aid of the characteristic velocity U^*, as this is given through the constant mass flow-rate at the exit of the tube, Eq. 11. Thus, it is more appropriate to define new parameters, $\hat{\varepsilon}$ and $\widehat{We}$, that depend only on the fluid properties and the dimensions of the tube:

$$\hat{\varepsilon} \equiv \frac{8\varepsilon^*\left(\eta_s^* + \eta_p^*\right)^2 L^{*2}}{\rho_0^* R^{*4}}, \quad \widehat{We} \equiv \frac{\lambda^*\left(\eta_s^* + \eta_p^*\right)}{\rho_0^* R^{*3}} \tag{50}$$

For the new parameters, it is trivial to show that $\varepsilon = \hat{\varepsilon}\widehat{Re}$ and $We = \widehat{We}\widehat{Re}$. Substituting the latter expressions in Eqs. 42, 43, and 48, we get $\Delta\left\langle -p\right\rangle$, $\Delta\left\langle \hat{T}_{zz}\right\rangle$ and $Re\overline{f}/32$, respectively, as functions of $\hat{\varepsilon}$ and $\widehat{We}$ (in addition to the already presented parameters $\widehat{Re}$, η_p, and a). In Fig. 5, we plot the pressure drop $\Delta\left\langle -p\right\rangle$ and $Re\overline{f}/32$ as functions of the modified Reynolds number $\widehat{Re}$ for $\hat{\varepsilon} = 0.4,\ 1$, and 10, for a Newtonian fluid ($\widehat{We} = 0$) and a viscoelastic fluid with $\widehat{We} = 0.3$. The modified Reynolds number varies from zero up to a critical value, $\widehat{Re}_c$, so that $0 \le \varepsilon \le \varepsilon_c$, and is calculated as follows. From $0 \le \varepsilon \le \varepsilon_c$ and the definition for $\hat{\varepsilon}$ we get $0 \le \widehat{Re} \le \widehat{Re}_c$. Then, by virtue of the relation $\varepsilon_c = 1/(2c)$, where c is given by Eq. 35, we obtain

$$\hat{\varepsilon}\left(\frac{1}{2} - \frac{56}{9}\eta_p\widehat{We}\right)\widehat{Re}_c^2 - \hat{\varepsilon}\left(3 - \frac{a^2}{9}\right)\widehat{Re}_c + 1 = 0 \tag{51}$$

the acceptable solution of which is

$$\widehat{Re}_c = \frac{1}{1 - \frac{112}{9}\eta_p\widehat{We}} \times\left\{3 - \frac{a^2}{9} - \sqrt{\left(3 - \frac{a^2}{9}\right)^2 + \frac{1}{\hat{\varepsilon}}\left(\frac{224}{9}\eta_p\widehat{We} - 2\right)}\right\} \tag{52}$$

Therefore, for specific values of a, $\hat{\varepsilon}$, $\widehat{We}$, and η_p the perturbation solution is valid up to the critical Reynolds number given by Eq. 52. For a Newtonian fluid ($We = 0$) and a long tube, $a << 1$, Eq. 52 reduces to $Re_c \approx 3 - \sqrt{9 - 2/\hat{\varepsilon}}$. The results shown in Fig. 6 reveal that the trend in viscoelastic flow is opposite to that of the Newtonian flow, since $\Delta\left\langle -p\right\rangle$ decreases with the presence of viscoelasticity while $Re\overline{f}/32$ increases. This justifies our abovementioned assertion that $Re\overline{f}/32$ and $\Delta\left\langle -p\right\rangle$ are different, especially in the viscoelastic case.

On the validity of the one-dimensional and lubrication approximations

For the one-dimensional approximation the assumption $\left\langle \rho u_z^2\right\rangle \approx \left\langle \rho\right\rangle\left\langle u_z\right\rangle^2$ is usually made (Shapiro 1953; Schwartz 1987; Venerus 2006). Schwartz (1987) and Venerus (2006) showed that for laminar flow, this assumption results in the incorrect prediction for the friction factor at the leading-order effect of compressibility. Indeed, using the analytical solution derived here, Eqs. 25a, b and 26a, b, we find

$$\Delta\left(\left\langle \rho u_z^2\right\rangle\right) = \Delta\left(\left\langle \rho\right\rangle\left\langle u_z\right\rangle^2\right) + \varepsilon\frac{1}{3} - \varepsilon^2\left(\frac{1}{2} + \frac{\widehat{Re}}{60} + \frac{20}{9}\eta_p We\right) + O\left(\varepsilon^3\right) \tag{53}$$

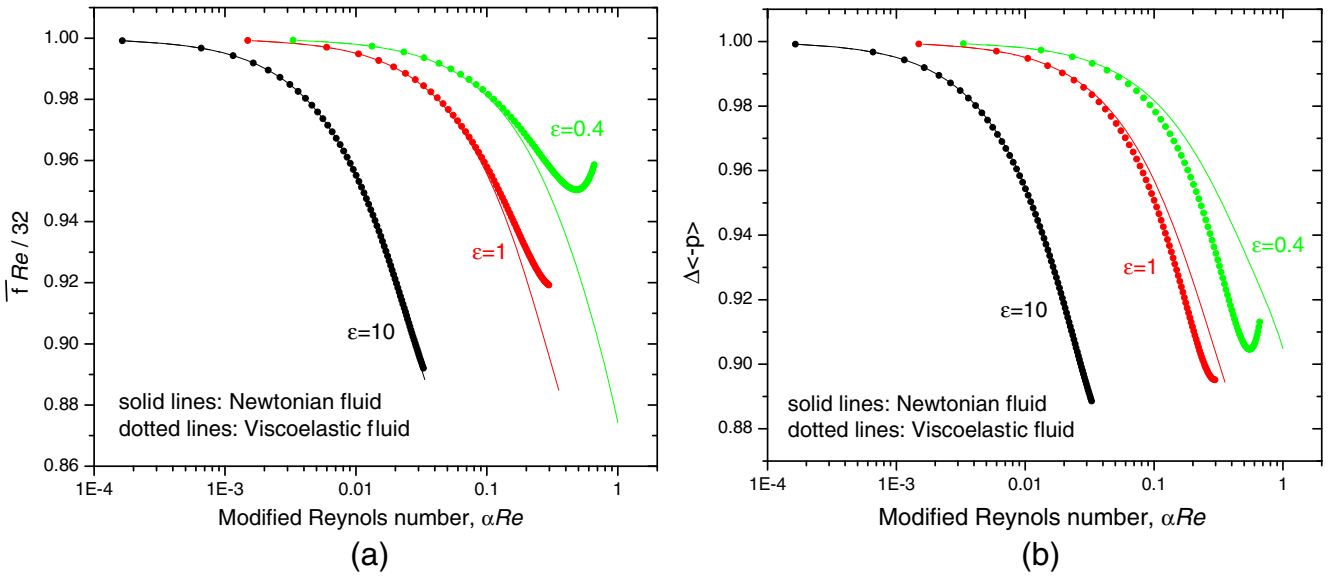

Fig. 6 The friction factor **a** and the pressure drop **b**, for a Newtonian $\left(\widehat{We}=0\right)$ and a viscoelastic fluid $(\widehat{We}=0.3)$ as functions of $\widehat{Re}=a\,Re$, for $\widehat{\varepsilon}=0.4,\ 1.0,$ and 10. Results are shown for values of $\widehat{Re}$ such that $\varepsilon \leq \varepsilon_c$

Hence, the error of the one-dimensional approximation is of first order and therefore an erroneous friction factor results which in this case takes the form:

$$\frac{Re}{32}\overline{f}=1-\varepsilon\left(\frac{1}{2}-\frac{1}{8}\widehat{Re}-\frac{8}{9}\eta_p We\right)+O\left(\varepsilon^2\right) \tag{54}$$

Clearly, the error comes from the combined effect of compressibility with inertia, while the one-dimensional approximation affects the contribution of the fluid viscoelasticity on the skin friction only at higher orders.

Regarding the lubrication approximation, the assumptions made implicitly or explicitly are $u_r=0$ and $\partial p/\partial r=0$. As Eq. 27a, b shows, the former induces an $O(\varepsilon^2)$ error while the latter induces an $O(\varepsilon)$ error. Indeed, by means of Eq. 26a, b, the pressure gradient in the radial direction is

$$\begin{aligned}\frac{\partial p}{\partial r}=&-\frac{1}{6}a^2\varepsilon r\\&\times\left(1+\varepsilon\left\{\frac{\widehat{Re}}{6}\left(9-15r^2+5r^4\right)\right.\right.\\&\left.\left.+\frac{12}{27}\eta_p We\left(43-66r^2\right)-3\left(1-z\right)\right\}\right)\\&+O\left(\varepsilon^3\right)\end{aligned} \tag{55}$$

Clearly, the first order error in the pressure gradient is a combination of fluid compressibility with viscous forces. For long tubes or capillaries, i.e., for $a<<1$, the radial pressure gradient at $O(\varepsilon)$ can be safely ignored since $a^2\varepsilon/6<<1$; same holds at $O(\varepsilon^2)$ even for high values of the Reynolds and/or Weissenberg numbers, provided that the flow remains laminar.

Primary flow variables

Here we discuss further the solution for the primary flow variables, e.g., the velocity, the pressure, and the stress fields. From Eq. 26a, b, it is deduced that the axial velocity component, u_z, deviates from the parabolic incompressible profile at first order, due to fluid inertia and viscoelasticity. The deviations at various axial positions for a Newtonian and viscoelastic fluid ($We=0.2$) and $Re=1$ are shown in Fig. 7a. The compressibility parameter was chosen to be rather high ($\varepsilon=0.25$) in order to magnify the differences. The effect of viscoelasticity is reduced with the radial coordinate. Analogous results for the radial velocity component, u_r, are shown in Fig. 7b. According to Eq. 27a, b, u_r varies linearly with the Weissenberg and the Reynolds numbers. Similar observations have been made earlier for the plane Newtonian Poiseuille flow (Housiadas and Georgiou 2011).

Deviations from the parabolic profile and the radial velocity component are induced by pressure gradients in both axial and radial directions. At zero order, the dimensionless pressure and its gradient do not depend on any dimensionless number of the flow problem. However, both *Re* and *We* contribute separately at first order and in combination at second order. It is worth

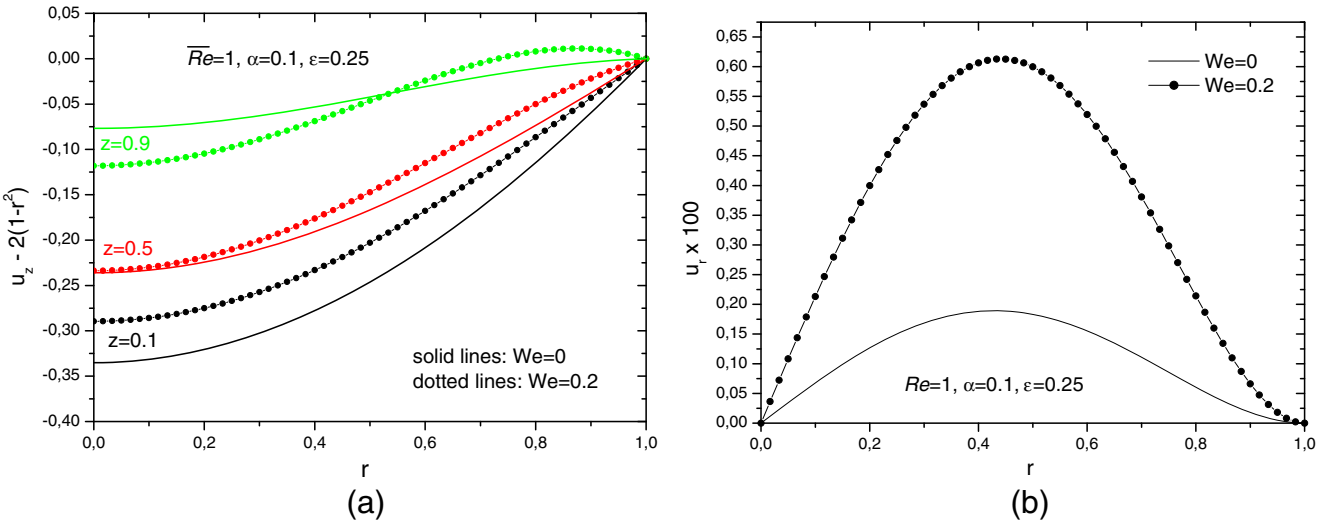

Fig. 7 The deviation of the velocity components from the incompressible velocity profile for a Newtonian ($We = 0$) and a viscoelastic fluid ($We = 0.2$) as functions of the radial distance from the center of the tube: **a** the axial velocity at $z = 0.1$, 0.5, and 0.9; **b** the radial velocity

mentioning that the combined effect of fluid compressibility with the viscous forces induces a non-zero radial pressure gradient at $O(\varepsilon)$ which does not depend on the axial position, as Eq. 55 shows, and most importantly, does not give rise to a radial velocity component. This is an indication that the perturbation solution is built up slowly as more terms in the perturbation expansion are calculated.

In Fig. 8, the pressure contours for a Newtonian fluid ($We = 0$) and a viscoelastic fluid ($We = 0.2$) with $\widehat{Re} = 1.0$ and $\varepsilon = 0.2$ are shown. The critical compressibility numbers are respectively $\varepsilon_c \approx 0.4$ and $\varepsilon_c \approx 0.277$. The effect of viscoelasticity is significant; although the contours are similar, almost vertical and equidistant, in the viscoelastic case they are shifted towards the entrance of the tube, in comparison to the Newtonian case. The shifting is less pronounced at the exit of the tube, which clearly shows that this is a combined compressibility/viscoelastic effect (see also Eq. 25a, b).

In Fig. 9, we show the axial velocity contours, which are horizontal in incompressible flow and curved towards the axis of symmetry in compressible flow. This

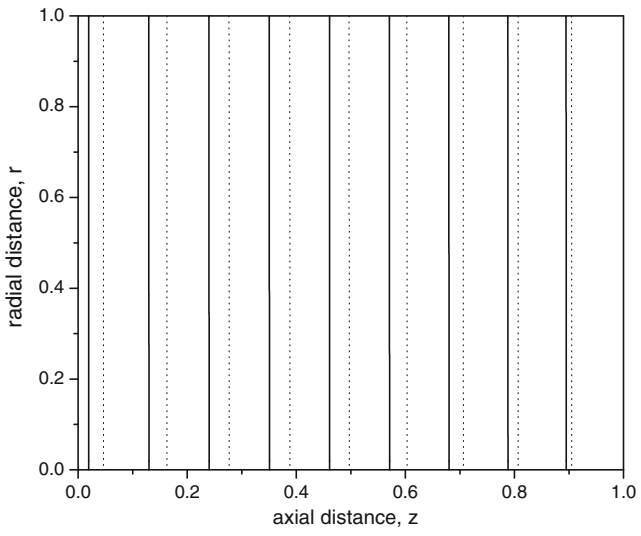

Fig. 8 Pressure contours for a Newtonian ($We = 0$, *dotted lines*) and a viscoelastic fluid ($We = 0.2$, *solid lines*); $\varepsilon = 0.2$ and $\widehat{Re} = 1.0$

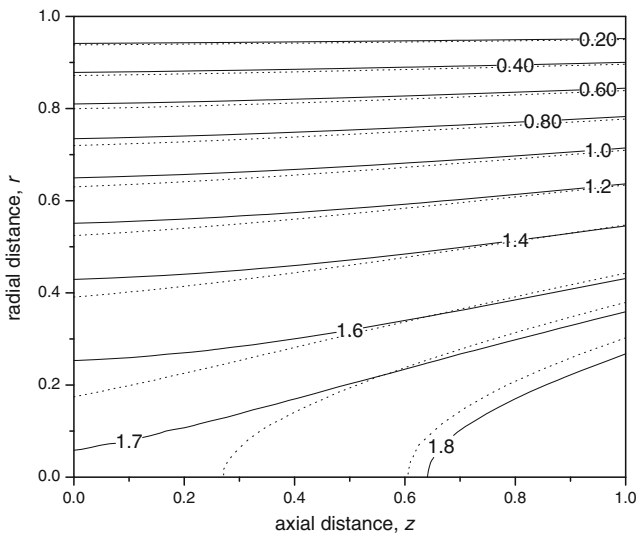

Fig. 9 Axial velocity for a Newtonian ($We = 0$, *dotted lines*) and a viscoelastic fluid ($We = 0.2$, *solid lines*); $\varepsilon = 0.2$ and $\widehat{Re} = 1$

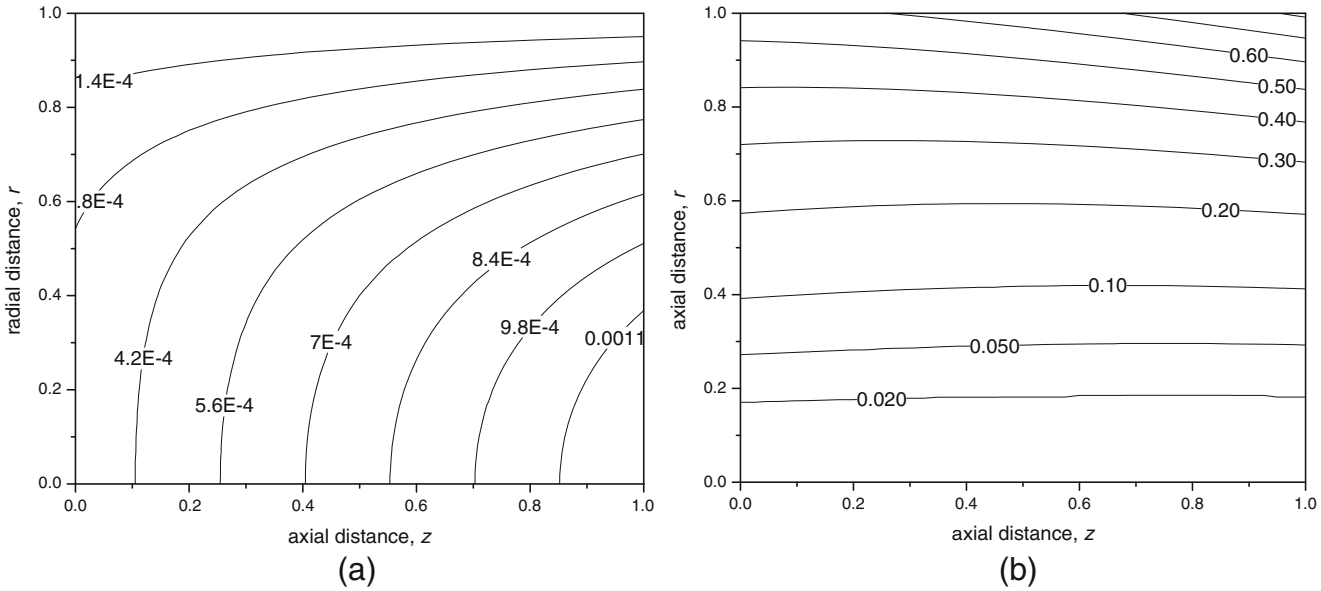

Fig. 10 Contours of the first normal stress difference, $\widehat{N}_1$, for **a** Newtonian fluid, $We = 0$, and **b** a viscoelastic fluid with $We = 0.2$; $\varepsilon = 0.2$, and $\widehat{Re} = 1$

is obviously due to the fact that for the mass to be preserved the flow accelerates downstream to counterbalance the reduction of the density. Finally, the contours for the first normal stress difference, $\widehat{N}_1$, for a Newtonian fluid ($We = 0$) and a viscoelastic fluid with $We = 0.2$ are shown in Fig. 10. In the Newtonian case, $\widehat{N}_1$ is small and its contours are bending towards the axis of symmetry, while in the viscoelastic case $\widehat{N}_1$ grows larger and its contours near the symmetry axis are almost horizontal.

As already mentioned, the second normal stress difference, N_2, is non-zero but very small in magnitude. The contours appear horizontal and the differences between the Newtonian and the viscoelastic case are very small. Similarly, the combined effect of fluid compressibility with viscoelasticity on $\hat{T}_{xy}$ appears to be weak. However, it should be mentioned that the magnitude of $\hat{T}_{xy}$ for the viscoelastic fluid is always less than the Newtonian one.

Conclusions

A perturbation solution for the laminar, isothermal, weakly compressible axisymmetric Poiseuille flow of an Oldroyd-B fluid in circular tubes and capillaries has been derived. The primary variables of the flow, namely the velocity, pressure, mass density, and polymer extra-stress fields, were expanded as power series of the compressibility number and the solution was obtained up to second order. Expressions for the volumetric flow rate, the pressure drop, and the friction factor have been obtained up to second order. The derived solution shows that fluid compressibility, inertia, and viscoelasticity have a significant effect on all the primary variables describing the flow. It was also demonstrated that the one-dimensional and lubrication approximations lead to erroneous predictions even at the leading-order effects of fluid compressibility. Last, it should be mentioned that in addition to the relevant applications, the analytical solution derived here may be useful for validation purposes for those developing numerical algorithms for viscoelastic compressible flows.

References

Belblidia F, Keshtiban IJ, Webster MF (2006) Stabilized computations for viscoelastic flows under compressible considerations. J Non-Newton Fluid Mech 134:56–76

Georgiou GC, Crochet MJ (1994a) Compressible viscous flow in slits with slip at the wall. J Rheol 38:639–654

Georgiou GC, Crochet MJ (1994b) Time-dependent compressible extrudate-swell problem with slip at the wall. J Rheol 38:1745–1755

Guillopé C, Hakim A, Talhouk R (2005) Existence of steady flows of slightly compressible viscoelastic fluids of White-Metzner type around an obstacle. Commun Pure Appl Anal 4:23–43

Guo ZY, Wu XB (1997) Compressibility effect on the gas flow and heat transfer in a microtube. Int J Heat Mass Transfer 40:3251–3254

Guo ZY, Wu XB (1998) Further study on compressibility effects on the gas flow and heat transfer in a microtube. Microscale Thermophys Eng 2:111–120

Harley C, Huang YH, Bau H, Zemel JN (1995) Gas flow in microchannels. J Fluid Mech 284:257–274
Hatzikiriakos SG, Dealy JM (1992) Role of slip and fracture in the oscillating flow of HDPE in a capillary. J Rheol 36:845–884
Hatzikiriakos SG, Dealy JM (1994) Start-up pressure gradients in a capillary rheometer. Polym Eng Sci 34:493–499
Housiadas KD, Georgiou GC (2011) Perturbation solution of a weakly compressible Oldroyd-B fluid. J Non-Newton Fluid Mech 166:73–92
Keshtiban IJ, Belblidia F, Webster MF (2004) Numerical simulation of compressible viscoelastic liquids. J Non-Newton Fluid Mech 122:131–146
Keshtiban IJ, Belblidia F, Webster MF (2005) Computation of incompressible and weakly-compressible viscoelastic liquids flow: finite element/volume schemes. J Non-Newton Fluid Mech 126:123–143
Mamoutos IG (2010) Analytical solution for the laminar flow of a weakly compressible fluid in a tube using perturbation methods. M.Sc. Thesis, Department of Mathematics, University of the Aegean, Samos, Greece
Mitsoulis E, Hatzikiriakos SG (2009) Steady flow simulations of compressible PTFE paste extrusion under severe wall slip. J Non-Newton Fluid Mech 157:26–33
Poinsot T, Lele S (1992) Boundary conditions for direct simulations of compressible viscous flows. J Comput Phys 101:104–129
Prud'homme RK, Chapman TW, Bowen JR (1986) Laminar compressible flow in a tube. Appl Sci Res 43:67–74
Ranganathan M, Mackley MR, Spitteler PHJ (1999) The application of the multipass rheometer to time-dependent capillary flow measurements of a polyethylene melt. J Rheol 43:443–451
Schwartz LW (1987) A perturbation solution for compressible viscous channel flows. J Eng Math 21:69–86
Shapiro AH (1953) The dynamics and the thermodynamics of compressible fluid flow, vol I. The Roland Press Co., New York
Taliadorou E, Georgiou GC, Alexandrou AN (2007) A two-dimensional numerical study of the stick–slip extrusion instability. J Non-Newton Fluid Mech 146:30–44
Taliadorou E, Georgiou GC, Mitsoulis E (2008) Numerical simulation of the extrusion of strongly compressible Newtonian liquids. Rheol Acta 47:49–62
Taliadorou EG, Neophytou M, Georgiou GC (2009a) Perturbation solutions of Poiseuille flows of weakly compressible Newtonian liquids. J Non-Newton Fluid Mech 163:25–34
Taliadorou E, Georgiou GC, Moulitsas I (2009b) Weakly compressible Poiseuille flows of a Herschel-Bulkley fluid. J Non-Newton Fluid Mech 158:162–169
Valette R, Mackley MR, Hernandez Fernandez del Castillo G (2006) Matching time dependent pressure driven flows with a Rolie Poly numerical simulation. J Non-Newton Fluid Mech 136:118–125
van den Berg HR, Seldam CA, van der Gulik PS (1993) Compressible laminar flow in a capillary. J Fluid Mech 246:1–20
Venerus DC (2006) Laminar capillary flow of compressible viscous fluids. J Fluid Mech 555:59–80
Venerus DC, Bugajsky DJ (2010) Compressible laminar flow in a channel. Phys Fluids 22:046101
Vinay G, Wachs A, Frigaard I (2006) Numerical simulation of weakly compressible Bingham flows: the restart of pipeline flows of waxy crude oils. J Non-Newton Fluid Mech 136:93–105
Webster MF, Keshtiban IJ, Belblidia F (2004) Computation of weakly compressible highly-viscous liquid flows. Eng Comput 21:777–804
Zohar Y, Lee SYK, Lee WY, Jiang L, Tong P (2002) Subsonic gas flow in a straight and uniform microchannel. J Fluid Mech 472:125–151